

Statistical Physics of Fracture and Earthquake

Bikas K. Chakrabarti

Theoretical Condensed Matter Physics Division and
Centre for Applied Mathematics and Computational Science,
Saha Institute of Nuclear Physics,
1/AF Bidhannagar, Kolkata 700064, India.

This chapter introduces the fracture nucleation process, their (extreme) statistics in disordered solids, in fiber bundle models, and in the two fractal overlap models of earthquake.

I. INTRODUCTION

A. Models of Fracture in Disordered Solids and Statistics

If one applies tensile stress on a solid, the solid elongates and gets strained. The stress (σ) - strain (ϵ) relation is linear for small stresses (Hooke's law) after which nonlinearity appears, in most cases. Finally at a critical stress σ_f , depending on the material, amount of disorder and the specimen size etc., the solid breaks into pieces; fracture occurs. In the case of brittle solids, the fracture occurs immediately after the Hookean linear region, and consequently the linear elastic theory can be applied to study the essentially nonlinear and irreversible static fracture properties of brittle solids [1]. With extreme perturbation, therefore, the mechanical or electrical properties of solids tend to get destabilised and failure or breakdown occurs. In fact, these instabilities in the solids often nucleate around disorder, which then plays a major role in the breakdown properties of the solids. The growth of these nucleating centres, in turn, depends on various statistical properties of the disorder, namely the scaling properties of percolating structures, its fractal dimensions, etc. These statistical properties of disorder induce some scaling behaviour for the breakdown of the disordered solids [2, 3].

Obviously with more and more random voids, the linear response of e.g. the modulus of elasticity Y (say, the Young's modulus) of the solid decreases. So also does the breaking strength of the material: the fracture strength σ_f of the specimen. For studying most of these mechanical (elastic) breakdown problems of randomly disordered solids, one can take the lattice model of disordered solids. In these lattice models, a fraction p of the bonds (or sites) are intact, with the rest $(1-p)$ being randomly broken or cut. Fluctuations in the random distribution give rise to random clusters of springs inside the bulk, for which the statistics is well developed [4], and one can investigate the effect of the voids or impurity clusters on the ultimate strength of the (percolating) elastic network of the bulk solid [2, 3]. One can also consider and compare the results for failure strength of the solids with random bond strength distribution, as for example, in random fiber bundle models (see e.g. [6, 7, 8]).

As is well known, the initial variations (decreases) of the linear responses like the elastic constant Y so the breakdown strengths σ_f is analytic with the impurity (dilution) concentration. Near the percolation threshold [4] p_c , up to (and at) which the solid network is marginally connected through the nearest neighbour occupied bonds or sites and below which the macroscopic connection ceases, the variations in these quantities with p are expected to become singular; the leading singularities being expressed by the respective critical exponents. The exponents for the modulus of elasticity $Y \sim p^{T_e}$ $p = (p - p_c) = p_c$ are well known and depend essentially on the dimension d of the system (see e.g., [4]). One kind of investigation searches for the corresponding singularities for the essentially nonlinear and irreversible properties of such mechanical breakdown strengths for p near the percolation threshold p_c : to find the exponent T_f for the average fracture stress

$\sigma_f \sim p^{T_f}$ for p near p_c . Very often, one maps [5] the problem of breakdown to the corresponding linear problem (assuming brittleness up to the breaking point) and then derives [2] the scaling relations giving the breakdown exponents T_f in terms of the linear response exponent (T_e) and other lattice statistical exponents (see next section).

Unlike that for the 'classical' linear responses of such solids, the extreme nature of the breakdown statistics, nucleating from the weakest point of the sample, gives rise to a non-self-averaging property. We will discuss (in the next section) these distribution functions $F(\sigma)$, giving the cumulative probability of failure of a disordered sample of

linear size L . We show that the generic form of the function $F(\sigma)$ can be either the Weibull [2] form

$$F(\sigma) = 1 - \exp\left[-\left(\frac{\sigma}{\sigma_0}\right)^d\right] \quad (1)$$

or the Gumbel [2] form

$$F(\sigma) = 1 - \exp\left[-\exp\left(\frac{\sigma}{\sigma_0}\right)\right] \quad (2)$$

where σ_0 is determined by the linear response like the elasticity of the disordered solid by some other lattice statistical quantity etc. and d is an exponent discussed in the next section.

In another kind of model for disordered systems, a loaded bundle of fibers represents the various aspects of fracture process through its self-organized dynamics. The fiber bundle model study was initiated by P. P. P. [6] in the context of testing the strength of cotton yarns. Since then, this model has been studied from various points of view. Fiber bundles are of two classes with respect to the time dependence of fiber strength: The 'static' bundles contain fibers whose strengths are independent of time, whereas the 'dynamic' bundles are assumed to have time dependent elements to capture the creep rupture and fatigue behaviors. For simplicity, we will discuss here the 'static' fiber bundle models only. According to the load sharing rule, fiber bundles are being classified into two groups: Equal load-sharing (ELS) bundles or democratic bundles and local load-sharing (LLS) bundles. In democratic or ELS bundles, intact fibers bear the applied load equally and in local load-sharing bundles the terminal load of the failed fiber is given equally to all the intact neighbors. The classic work of Daniels [7] on the strength of the static fiber bundles under equal load sharing (ELS) assumption initiated the probabilistic analysis of the model (see e.g., [8]). The distribution of burst avalanches during fracture process is a marked feature of the fracture dynamics and can be observed in ultrasonic emissions during the fracture process. It helps characterizing different physical systems along with the possibility to predict the large avalanches. From a nontrivial probabilistic analysis, one gets [9] power law distribution of avalanches for static ELS bundles, whereas the power law exponent observed numerically for static LLS bundles differs significantly. This observation induces the possibility of presenting loaded fiber bundles as earthquake models (see Sec. 3). The phase transition [8] and dynamic critical behavior of the fracture process in such bundles has been established through recursive formulation [8, 10] of the failure dynamics. The exact solutions [10] of the recursion relations suggest universal values of the exponents involved. A attempt has also been made [11] to study the ELS and LLS bundles from a single framework introducing a 'range of interaction' parameter which determines the load transfer rule.

B. Earthquake Models and Statistics

The earth's solid outer crust, of about 20 kilometers in average thickness, rests on the tectonic shells. Due to the high temperature-pressure phase changes and the consequent powerful convective flow in the earth's mantle, at several hundreds of kilometers of depth, the tectonic shell, divided into a small number (about ten) of mobile plates, has relative velocities of the order of a few centimeters per year [12, 13]. Over several tens of years, enormous elastic strains develop sometimes on the earth's crust when sticking (due to the solid-solid friction) to the moving tectonic plate. When slips occur between the crust and the tectonic plate, these stored elastic energies are released in 'bursts', causing the damages during the earthquakes. Because of the uniform motion of the tectonic plates, the elastic strain energy stored in a portion of the crust (block), moving with the plate relative to a 'stationary' neighbouring portion of the crust, can vary only due to the random strength of the solid-solid friction between the crust and the plate. The slip occurs when the accumulated stress exceeds the frictional force.

As in fracture (in fiber bundle model in particular), the observed distribution of the elastic energy release in various earthquakes seems to follow a power law. The number of earthquakes $N(m)$, having magnitude in the Richter scale greater than or equal to m , is phenomenologically observed to decrease with m exponentially. This gives the Gutenberg-Richter law [12]

$$\ln N(m) = \text{constant} - a m;$$

where a is a constant. It appears [12, 13] that the amount of energy released in an earthquake of magnitude m is related to it exponentially:

$$\ln E = \text{constant} + b m;$$

where b is another constant. Combining therefore we get the power law giving the number of earthquakes $N(E)$ releasing energy equal to E as

$$N(E) \propto E^{-\alpha}; \quad (3)$$

with $\alpha = \beta$. The observed value of the exponent (power) in (3) is around unity (see e.g., [13]).

Several laboratory and computer simulation models have recently been proposed [2] to capture essentially the above power law in the earthquake energy release statistics. In a very successful table-top laboratory simulation model of earthquakes, Burridge and Knopoff [14] took a chain of wooden blocks connected by identical springs to the neighbouring blocks. The entire chain was placed on a rigid horizontal table with a rough surface, and one of the end blocks was pulled very slowly and uniformly using a driving motor. The strains of the springs increase due to the creep motions of the blocks until one or a few of the blocks slip. The drops in the elastic energy of the chain during slips could be measured from the extensions or compressions of all the springs, and could be taken as the released energies in the earthquake. For some typical roughness of the surfaces (of the blocks and of the table), the distribution of these drops in the elastic energy due to slips indeed shows a power law behaviour with $\alpha \approx 1$ in (3).

A computer simulation version of this model by Carlson and Langer [15] considers harmonic springs connecting equal mass blocks which are also individually connected to a rigid frame (to simulate other neighbouring portions of the earth's crust not on the same tectonic plate) by harmonic springs. The entire system moves on a rough surface with nonlinear velocity dependent force (decreasing to zero for large relative velocities) in the direction opposite to the relative motion between the block and the surface. In the computer simulation of this model it is seen that the distribution of the elastic energy release in such a system can indeed be given by a power law like (3), provided the nonlinearity of the friction force, responsible for the self-organisation, is carefully chosen [15].

The lattice automaton model of Bak et al [16] represent the stress on each block by a height variable at each lattice site. The site topples (the block slips) if the height (or stress) at that site exceeds a preassigned threshold value, and the height becomes zero there and the neighbours share the stress by increasing their heights by one unit. With this dynamics for the system, if any of the neighbouring sites of the toppled one was already at the threshold height, the avalanche continues. The boundary sites are considered to be all absorbing. With random addition of heights at a constant rate (increasing stress at a constant rate due to tectonic motion), such a system reaches its self-organised critical point where the avalanche size distributions follow a natural power law corresponding to this self-tuned critical state. Bak et al [16] identify this self-organised critical state to be responsible for the Gutenberg-Richter type power law. All these models are successful in capturing the Gutenberg-Richter power law, and the real reason for the self-similarity inducing the power law is essentially the same in all these different models: emergence of the self-organised critical state for wide yet suitably chosen variety of nonlinear many-body coupled dynamics. In this sense all these models incorporate the well-established fact of the stick-slip frictional instabilities between the earth's crust and the tectonic plate. It is quite difficult to check at this stage any further details and predictions of these models.

While the motion of the tectonic plate is surely an observed fact, and this stick-slip process should be a major ingredient of any bona fide model of earthquake, another established fact regarding the fault geometries of the earth's crust is the fractal nature of the roughness of the surfaces of the earth's crust and the tectonic plate. This latter feature is missing in any of these models discussed above. In fact, the surfaces involved in the process are results of large scale fracture separating the crust from the moving tectonic plate. Any such crack surface is observed to be a self-similar fractal, having the self-affine scaling property $z(x; y) \sim z(x; y)$ for the surface coordinate z in the direction perpendicular to the crack surface in the $(x; y)$ plane [2]. Various fractographic investigations indicate a fairly robust universal behaviour for such surfaces and the roughness exponent is observed to have a value around $0.80 - 0.85$ (with a possible crossover to $\alpha \approx 0.4$ for slow propagation of the crack-tip) [2, 3]. This widely observed scaling property of the fracture surfaces also suggests that the fault surfaces of the earth's crust or the tectonic plate should have similar fractal properties. In fact, some investigators of the earthquake dynamics have already pointed out that the fracture mechanics of the stressed crust of the earth forms self-similar fault patterns, with well-defined fractal dimensionalities near the contact areas with the major plates [2]. Based on these observations regarding the earthquake faults, we have developed a 'two-fractal overlap' model [17, 18] discussed later.

II. FRACTURE STATISTICS OF DISORDERED SOLIDS

A. Grith Energy Balance and Brittle Fracture Strength of Solids

One can easily show (see e.g. [1, 2]) that in a stressed solid, the local stress at sharp notches or corners of the microcrack can rise to a level several times that of the applied stress. This indicates how the microscopic cracks or flaws within a solid might become potential sources of weakness of the solid. Although this stress concentration indicates clearly where the instabilities should occur, it is not sufficient to tell us when the instability does occur and the fracture propagation starts. This requires a detailed energy balance consideration.

Grith in 1920, equating the released elastic energy (in an elastic continuum) with the energy of the surface newly created (as the crack grows), arrived at a quantitative criterion for the equilibrium extension of the microcrack already present within the stressed material [19]. We give below an analysis which is valid effectively for two-dimensional stressed solids with a single pre-existing crack, as for example the case of a large plate with a small thickness. Extension

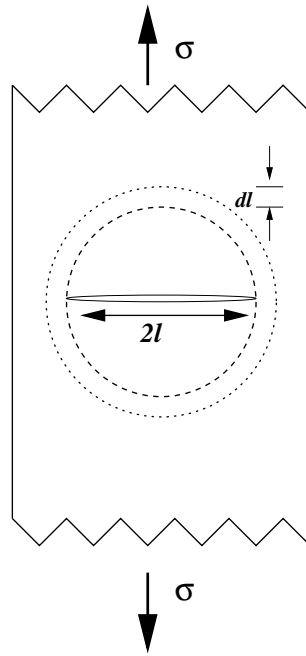


FIG. 1: A portion of a plate (of thickness w) under tensile stress (Model I loading) containing a linear crack of length $2l$. For a further growth of the crack length by $2dl$, the elastic energy released from the annular region must be sufficient to provide the surface energy $4w\gamma dl$ (extra elastic energy must be released for finite velocity of crack propagation).

to three-dimensional solids is straightforward.

Let us assume a thin linear crack of length $2l$ in an infinite elastic continuum subjected to uniform tensile stress σ perpendicular to the length of the crack (see Fig. 1). Stress parallel to the crack does not affect the stability of the crack and has not, therefore, been considered. Because of the crack (which can not support any stress field, at least on its surfaces), the strain energy density of the stress field ($\sigma^2/2Y$) is perturbed in a region around the crack, having dimension of the length of the crack. We assume here this perturbed or stress-released region to have a circular cross-section with the crack length as the diameter. The exact geometry of this perturbed region is not important here, and it determines only an (unimportant) numerical factor in the Griffith formula (see e.g. [1]). Assuming therefore half of the stress energy of the annular or cylindrical volume, having the internal radius l and outer radius $l+dl$ and length w (perpendicular to the plane of the stress; here the width w of the plate is very small compared to the other dimensions), to be released as the crack propagates by a length dl , one requires this released strain energy to be sufficient for providing the surface energy of the four new surfaces produced. This suggests

$$\frac{1}{2} (\sigma^2/2Y) (2w\pi dl) = 4w\gamma dl \quad (4)$$

Here Y represents the Young's modulus of the solid and γ represents the surface energy density of the solid, measured by the extra energy required to create unit surface area within the bulk of the solid.

We have assumed here, on average, half of the strain energy of the cylindrical region having a circular cross-section with diameter $2l$ to be released. If this fraction is different or the cross-section is different, it will change only some of the numerical factors, in which we are not very much interested here. Also, we assume here linear elasticity up to the breaking point, as in the case of brittle materials. The equality holds when energy dissipation, as in the case of plastic deformation or for the propagation dynamics of the crack, does not occur. One then gets

$$\sigma_f = \frac{2\sqrt{2}\gamma}{2l}; \quad \sigma_f = \frac{2\sqrt{2}\gamma}{Y} \quad (4)$$

for the critical stress at and above which the crack of length $2l$ starts propagating and a macroscopic fracture occurs. Here σ_f is called the stress-intensity factor or the fracture toughness. In fact, one can alternatively view the fracture occurring when the stress at the crack-tip (given by the stress intensity factor in (4)) exceeds the elastic stress limit for the medium.

In a three-dimensional solid containing a single elliptic disk-shaped planar crack perpendicular to the applied tensile stress direction, a straightforward extension of the above analysis suggests that the maximum stress concentration

would occur at the two tips (at the two ends of the major axis) of the ellipse. The Griffith stress for the brittle fracture of the solid would therefore be determined by the same formula (4), with the crack length $2l$ replaced by the length of the major axis of the elliptic planar crack. Generally, for any dimension therefore, if a crack of length l already exists in an infinite elastic continuum, subject to uniform tensile stress perpendicular to the length of the crack, then for the onset of brittle fracture, Griffith equates (the differentials of) the elastic energy E_1 with the surface energy E_s :

$$E_1' = \frac{\sigma^2}{2Y} l^d = E_s' = \gamma l^{d-1}; \quad (5)$$

where Y represents the elastic modulus appropriate for the strain, γ the surface energy density and d the dimension. Equality holds when no energy dissipation (due to plasticity or crack propagation) occurs and one gets

$$\sigma_f = \left(\frac{2\gamma}{Y l} \right)^{1/d}; \quad (6)$$

for the breakdown stress at (and above) which the existing crack of length l starts propagating and a macroscopic fracture occurs. It may also be noted that the above formula is valid in all dimensions ($d \geq 2$).

For disordered solids, let us model the solid by a percolating system. As mentioned earlier, for the occupied bond/site concentration $p > p_c$, the percolation threshold, the typical pre-existing cracks in the solid will have the dimension (l) of correlation length $\xi \sim p^{-1}$ and the elastic strength $Y \sim p^{T_e}$ [4]. Assuming that the surface energy density scales as $\gamma \sim p^{d_B}$, with the backbone (fractal) dimension d_B [4], equating E_1 and E_s as in (5), one gets $\frac{\sigma_f^2}{2Y} l^d \sim p^{d_B}$. This gives

$$\sigma_f \sim (p)^{T_f}$$

with

$$T_f = \frac{1}{2} [T_e + (d - d_B)] \quad (7)$$

for the 'average' fracture strength of a disordered solid (of fixed value) as one approaches the percolation threshold. Careful extensions of such scaling relations (7) and rigorous bounds for T_f has been obtained and compared extensively in [2, 3].

B. Extreme Statistics of The Fracture Stress

The fracture strength σ_f of a disordered solid does not have self-averaging statistics; most probable and the average σ_f may not match because of the extreme nature of the statistics. This is because, the 'weakest point' of a solid determines the strength of the entire solid, not the average weak points! As we have modelled here, the statistics of clusters of defects are governed by the random percolation processes. We have also discussed, how the linear responses, like the elastic moduli of such random networks, can be obtained from the averages over the statistics of such clusters. This was possible because of the self-averaging property of such linear responses. This is because the elasticity of a random network is determined by all the 'parallel' connected material portions or paths, contributing their share in the net elasticity of the sample. However, the fracture or breakdown property of a disordered solid is determined by only the weakest (often the longest) defect cluster or crack in the entire solid. Except for some indirect effects, most of the weaker or smaller defects or cracks in the solid do not determine the breakdown strength of the sample. The fracture or breakdown statistics of a solid sample is therefore determined essentially by the extreme statistics of the most dangerous or weakest (largest) defect cluster or crack within the sample volume.

We discuss now more formally the origin of this extreme statistics. Let us consider a solid of linear size L , containing n cracks within its volume. We assume that each of these cracks have a failure probability $f_i(\sigma)$; $i = 1; 2; \dots; n$ to fail or break (independently) under an applied stress σ on the solid, and that the perturbed or stress-released regions of each of these cracks are separate and do not overlap. If we denote the cumulative failure probability of the entire sample, under stress σ , by $F(\sigma)$ then [2]

$$1 - F(\sigma) = \prod_{i=1}^n (1 - f_i(\sigma)) \quad \text{or} \quad \ln(1 - F(\sigma)) = - \sum_{i=1}^n f_i(\sigma) = - \int_0^L \rho(\sigma) dV \quad (8)$$

where $\rho(\sigma)$ denotes the density of cracks within the sample volume L^d (coming from the sum $\sum_{i=1}^n$ over the entire volume), which starts propagating at and above the stress level σ . The above equation comes from the fact that the

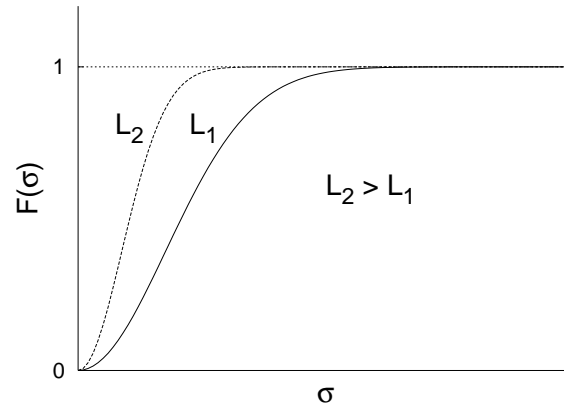


FIG. 2: Schematic variation of failure probability $F(\sigma)$ with stress σ for a disordered solid with volume L_1^d or L_2^d ($L_2 > L_1$).

sample survives if each of the cracks within the volume survives. This is the essential origin of the above extreme statistical nature of the failure probability $F(\sigma)$ of the sample.

Noting that the pair correlation $g(l)$ of two occupied sites at distance l on a percolation cluster decays as $\exp(-l/\xi(p))$, and connecting the stress σ with the length l by using Griffith's law (4) that $\sigma \propto l^{-1/2}$, one gets $g(\sigma) \propto \exp(-\frac{1}{\sigma^2})$ for $p \neq p_c$. This, put in eqn. (8) gives the Gumbel distribution (2) given earlier [2]. If, on the other hand, one assumes a power law decay of $g(l)$: $g(l) \propto l^{-w}$, then using the Griffith's law (4), one gets $g(\sigma) \propto \sigma^{-m}$, giving the Weibull distribution (1), from eqn. (8), where $m = w - 1$ gives the Weibull modulus [2]. The variation of $F(\sigma)$ with σ in both the cases have the generic form shown in Fig. 2. $F(\sigma)$ is non-zero for any stress $\sigma > 0$ and its value (at any σ) is higher for larger volume (L^d). This is because, the possibility of a larger defect (due to fluctuation) is higher in a larger volume and consequently, its failure probability is higher. Assuming $F(\sigma_f)$ is finite for failure, the most probable failure stress σ_f becomes a decreasing function of volume if extreme statistics at work.

The precise ranges of the validity of the Weibull or Gumbel distributions for the breakdown strength of disordered solids are not well established yet. However, analysis of the results of detailed experimental and numerical studies of breakdown in disordered solids seem to suggest that the fluctuations of the extreme statistics dominate for small disorder [3]. Very near to the percolation point, the percolation statistics takes over and the statistics become self-averaging. One can argue [19], that arbitrarily close to the percolation threshold, the fluctuations of the extreme statistics will probably get suppressed and the percolation statistics should take over and the most probable breaking stress becomes independent of the sample volume (its variation with disorder being determined, as in Eqn.(7), by an appropriate breakdown exponent). This is because the appropriate competing length scales for the two kinds of statistics are the Lifshitz scale $\ln L$ (coming from the finiteness of the volume integral of the defect probability: $L^d(1-p)^{1-\nu}$ finite, giving the typical defect size $l \sim \ln L$) and the percolation correlation length ξ . When $\xi < \ln L$, the above scenario of extreme statistics should be observed. For $\xi > \ln L$, the percolation statistics is expected to dominate.

C. Failure Statistics in Fiber Bundles

The fiber bundle (see Fig. 3) consists of N fibers or Hook springs, each having identical spring constant k . The bundle supports a load $W = Nkx$ and the breaking threshold $(\sigma_{th})_i$ of the fibers are assumed to be different for different fiber (i). For the equal load sharing model we consider here, the lower platform is absolutely rigid, and therefore no local deformation and hence no stress concentration occurs anywhere around the failed fibers. This ensures equal load sharing, i.e., the intact fibers share the applied load W equally and the load per fiber increases as more and more fibers fail. The strength of each of the fiber $(\sigma_{th})_i$ in the bundle is given by the stress value it can bear, and beyond which it fails. The strength of the fibers are taken from a randomly distributed normalised density $\rho(\sigma_{th})$ within the interval 0 and 1 such that

$$\int_0^1 \rho(\sigma_{th}) d\sigma_{th} = 1:$$

The equal load sharing assumption neglects 'local' fluctuations in stress (and its redistribution) and renders the model as a mean-field one.

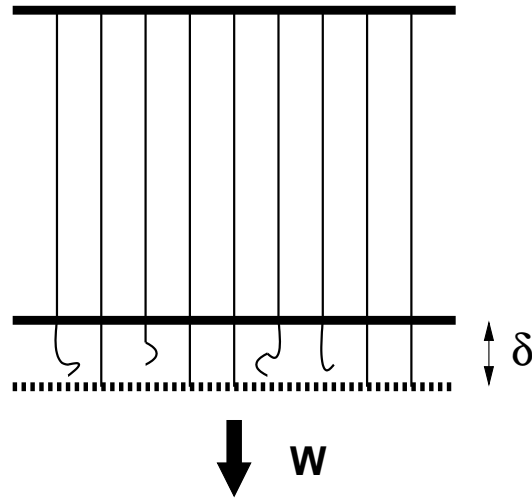


FIG .3: The fiber bundle consists initially of N fibers attached in parallel to a fixed and rigid plate at the top and a downwardly movable platform from which a load W is suspended at the bottom . In the equal load sharing model considered here, the platform is absolutely rigid and the load W is consequently shared equally by all the intact fibers.

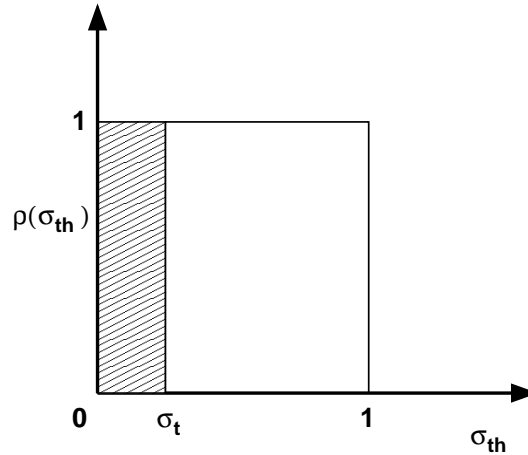


FIG .4: The simple model considered here assumes uniform density $\rho(\sigma_{th})$ of the fiber strength distribution up to a cut-off strength (normalized to unity). At any load per fiber level σ_t at time t , the fraction σ_t fails and $1 - \sigma_t$ survives.

The breaking dynamics starts when an initial stress (load per fiber) is applied on the bundle. The fibers having strength less than σ_t fail instantly. Due to this rupture, total number of intact fibers decreases and rest of the (intact) fibers have to bear the applied load on the bundle. Hence effective stress on the fibers increases and this compels some more fibers to break. These two sequential operations, namely the stress redistribution and further breaking of fibers continue till an equilibrium is reached, where either the surviving fibers are strong enough to bear the applied load on the bundle or all fibers fail.

This breaking dynamics can be represented by recursion relations in discrete time steps. For this, let us consider a very simple model of fiber bundles where the fibers (having the same spring constant k) have a white or uniform strength distribution $\rho(\sigma_{th})$ upto a cut-off strength normalized to unity, as shown in Fig. IIC: $\rho(\sigma_{th}) = 1$ for $0 \leq \sigma_{th} \leq 1$ and $\rho(\sigma_{th}) = 0$ for $\sigma_{th} > 1$. Let us also define $U_t(\sigma)$ to be the fraction of fibers in the bundle that survive after (discrete) time step t , counted from the time $t = 0$ when the load is put (time step indicates the number of stress redistributions). As such, $U_t(\sigma = 0) = 1$ for all t and $U_t(\sigma) = 1$ for $t = 0$ for any σ ; $U_t(\sigma) = 0$ for $t \geq 1$ and $\sigma < \sigma_c$, the critical or failure strength of the bundle, and $U_t(\sigma) = 0$ for $t \geq 1$ if $\sigma > \sigma_c$.

Therefore $U_t(\sigma)$ follows a simple recursion relation (see Fig. IIC)

$$U_{t+1}(\sigma) = 1 - \sigma_t; \quad \sigma_t = \frac{W}{U_t N}$$

$$\text{or; } U_{t+1} = 1 - \frac{U_t}{U_t} \quad (9)$$

At the equilibrium state ($U_{t+1} = U_t = U$), the above relation takes a quadratic form of U :

$$U^2 - U + \frac{1}{2} = 0:$$

The solution is

$$U(\sigma) = \frac{1}{2} \left(\sigma - \sigma_c \right)^{1/2}; \quad \sigma_c = \frac{1}{4}:$$

Here σ_c is the critical value of initial applied stress beyond which the bundle fails completely. The solution with (+) sign is the stable one, whereas the one with (-) sign gives unstable solution [10]. The quantity $U(\sigma)$ must be real valued as it has a physical meaning: it is the fraction of the original bundle that remains intact under a fixed applied stress σ when the applied stress lies in the range $0 < \sigma < \sigma_c$. Clearly, $U(0) = 1$. Therefore the stable solution can be written as

$$U(\sigma) = U(\sigma_c) + \left(\sigma - \sigma_c \right)^{1/2}; \quad U(\sigma_c) = \frac{1}{2} \text{ and } \sigma_c = \frac{1}{4} \quad (10)$$

For $\sigma > \sigma_c$ we can not get a real-valued fixed point as the dynamics never stops until $U_t = 0$ when the bundle breaks completely.

(a) At $\sigma < \sigma_c$

It may be noted that the quantity $U(\sigma) - U(\sigma_c)$ behaves like an order parameter that determines a transition from a state of partial failure ($\sigma < \sigma_c$) to a state of total failure ($\sigma > \sigma_c$) [10]:

$$0 < U(\sigma) - U(\sigma_c) = \left(\sigma - \sigma_c \right)^{1/2}; \quad \sigma_c = \frac{1}{4} \quad (11)$$

To study the dynamics away from criticality ($\sigma \neq \sigma_c$ from below), we replace the recursion relation (9) by a differential equation

$$\frac{dU}{dt} = \frac{U^2 - U + \frac{1}{2}}{U}:$$

Close to the fixed point we write $U_t(\sigma) = U(\sigma) + \delta U_t(\sigma)$ (where $\delta U_t \neq 0$). This, following Eq. (10), gives [10]

$$\delta U_t(\sigma) = \delta U_0(\sigma) \exp(-t/\tau); \quad (12)$$

where $\tau = \frac{1}{2} \frac{1}{\left(\sigma - \sigma_c \right)^{1/2}} + 1$. Near the critical point we can write

$$\tau \propto \left(\sigma - \sigma_c \right)^{-1}; \quad \sigma_c = \frac{1}{4} \quad (13)$$

Therefore the relaxation time diverges following a power-law as $\sigma \rightarrow \sigma_c$ from below [10].

One can also consider the breakdown susceptibility χ , defined as the change of $U(\sigma)$ due to an infinitesimal increment of the applied stress [10]

$$\chi = \frac{dU(\sigma)}{d\sigma} = \frac{1}{2} \left(\sigma - \sigma_c \right)^{-1/2}; \quad \sigma_c = \frac{1}{4} \quad (14)$$

from equation (10). Hence the susceptibility diverges as the applied stress approaches the critical value $\sigma_c = \frac{1}{4}$. Such a divergence in χ had already been observed in the numerical studies.

(b) At $\sigma = \sigma_c$

At the critical point ($\sigma = \sigma_c$), we observe a different dynamic critical behavior in the relaxation of the failure process. From the recursion relation (9), it can be shown that decay of the fraction $U_t(\sigma_c)$ of unbroken fibers that remain intact at time t follows a simple power-law decay [10]:

$$U_t = \frac{1}{2} \left(1 + \frac{1}{t+1} \right); \quad (15)$$

starting from $U_0 = 1$. For large t ($t \gg 1$), this reduces to $U_t \approx 1/2 + 1/(2(t+1))$; $\tau = 1$; a strict power law which is a robust characterization of the critical state.

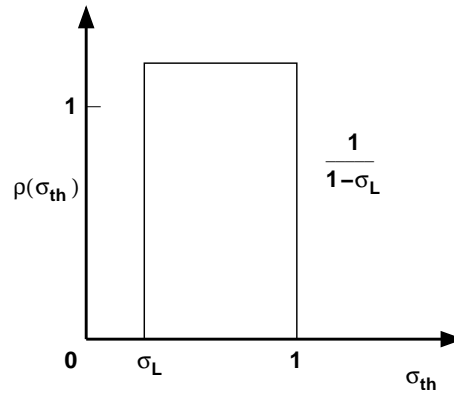


FIG. 5: The fiber breaking strength distribution (σ_{th}) considered for studying elastic-plastic type nonlinear deformation behavior of the equal load sharing model.

1. Universality Class of The Model

The universality class of the model has been checked [10] taking two other types of fiber strength distributions: (I) linearly increasing density distribution and (II) linearly decreasing density distribution within the (σ_{th}) limit 0 and 1. One can show that while σ_f changes with different strength distributions ($\sigma_f = \frac{1}{4} = 0.25$ for case (I) and $\sigma_f = \frac{1}{4} = 0.25$ for case II), the critical behavior remains unchanged: $\nu = 1 = 2 = \dots$, $\beta = 1$ for all these equal load sharing models.

2. Nonlinear Stress-Strain Relation for The Bundle

One can now consider a slightly modified strength distribution of the equal load sharing fiber bundle, showing typical nonlinear deformation characteristics [7, 10]. For this, we consider an uniform density distribution of fiber strength, having a lower cutoff σ_L . Until failure of any of the fibers (due to this lower cutoff), the bundle shows linear elastic behavior. As soon as the fibers start failing, the stress-strain relationship becomes nonlinear. The dynamic critical behavior remains essentially the same and the static (fixed point) behavior shows elastic-plastic like deformation before rupture of the bundle.

Here the fibers are elastic in nature having identical force constant and the random fiber strengths distributed uniformly in the interval $[\sigma_L; 1]$ with $\sigma_L > 0$; the normalized distribution of the threshold stress of the fibers thus has the form (see Fig. 5):

$$\rho(\sigma_{th}) = \begin{cases} 0; & 0 < \sigma_{th} < \sigma_L \\ \frac{1}{1-\sigma_L}; & \sigma_L < \sigma_{th} < 1 \end{cases} \quad (16)$$

For an applied stress σ_L none of the fibers break, though they are elongated by an amount $U = \sigma_L$. The dynamics of breaking starts when applied stress becomes greater than σ_L . Now, for $\sigma > \sigma_L$ the fraction of unbroken fibers follows a recursion relation (for $\rho(\sigma_{th})$ as in Fig. 5):

$$U_{t+1} = 1 - \frac{F}{N U_t} \left(\sigma - \sigma_L \right) \frac{1}{1-\sigma_L} = \frac{1}{1-\sigma_L} \left(1 - \frac{\sigma - \sigma_L}{U_t} \right); \quad (17)$$

which has stable fixed points:

$$U(\sigma) = \frac{1}{2(1-\sigma_L)} \left(1 + \frac{\sigma - \sigma_L}{\sigma_f} \right)^{\beta}; \quad \sigma_f = \frac{1}{4(1-\sigma_L)}; \quad (18)$$

The model now has a critical point $\sigma_f = 1/[4(1-\sigma_L)]$ beyond which total failure of the bundle takes place. The above equation also requires that $\sigma_L = 1/2$ (to keep the fraction $U < 1$). As one can easily see, the dynamics of U_t for $\sigma < \sigma_f$ and also at $\sigma = \sigma_f$ remains the same as discussed in the earlier section. At each fixed point there will be an equilibrium elongation $U(\sigma)$ and a corresponding stress $S = U(\sigma)$ develops in the system (bundle). This $U(\sigma)$ can be easily expressed in terms of $U(\sigma_f)$. This requires the evaluation of σ , the internal stress per fiber developed

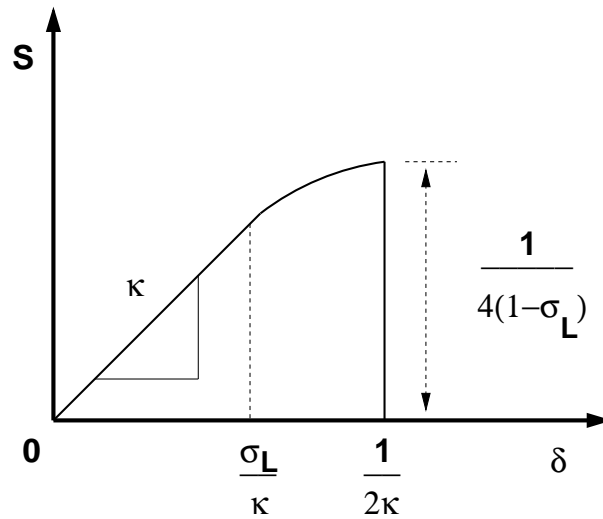


FIG .6: Schematic stress (S)-strain (δ) curve of the bundle (shown by the solid line), following Eq. (19), with the fiber strength distribution (16) (as shown in Fig. 5). Note, the model gives analytic solution for the full nonlinear stress-strain relationship of the bundle (disordered solid), including its failure (fracture) stress or strain.

at the fixed point, corresponding to the initial (external) stress ($= F/N$) per fiber applied on the bundle when all the fibers were intact. Expressing the effective stress per fiber in terms of $U(\delta)$, one can write from (17)

$$U(\delta) = 1 - \frac{\sigma_L}{1 - \sigma_L} \delta = \frac{1 - \sigma_L \delta}{1 - \sigma_L};$$

for $\delta > \sigma_L$. Consequently,

$$S(\delta) = \sigma_L U(\delta) = \frac{\sigma_L (1 - \sigma_L \delta)}{1 - \sigma_L};$$

It may be noted that the internal stress $\sigma_c (= \sigma_c U(\delta_c))$ is universally equal to $1/2$ (independent of σ_L ; from (18)) at the failure point $\delta = \delta_c$ of the bundle. This finally gives the stress-strain relation for the model:

$$S = \begin{cases} \sigma_L \delta & ; \delta \leq \sigma_L \\ \frac{\sigma_L (1 - \sigma_L \delta)}{1 - \sigma_L} & ; \sigma_L < \delta < \frac{1}{\sigma_L} \\ 0 & ; \delta \geq \frac{1}{\sigma_L} \end{cases} \quad (19)$$

This stress-strain relation is schematically shown in Fig. 6, where the initial linear region has slope σ_L (the force constant of each fiber). This Hooke's region for stress S continues up to the strain value $\delta = \sigma_L$, until which no fibers break ($U(\delta) = 1$). After this, nonlinearity appears due to the failure of a few of the fibers and the consequent decrease of $U(\delta)$ (from unity). It finally drops to zero discontinuously by an amount $\sigma_L U(\delta_f) = 1 - \sigma_L \delta_f$ at the breaking point $\delta = \delta_f$ or $\delta = \delta_f = 1/\sigma_L$ for the bundle. This indicates that the stress drop at the final failure point of the bundle is related to the extent (σ_L) of the linear region of the stress-strain curve of the same bundle.

3. Strength of The Local Load Sharing Fiber Bundles

So far, we studied models with fibers sharing the external load equally. This type of model shows (both analytically and numerically) existence of a critical strength (non zero σ_c) of the macroscopic bundle [10] beyond which it collapses. The other extreme model, i.e., the local load sharing model has been proved to be difficult to tackle analytically.

It is clear, however, that the extreme statistics comes into play for such local load sharing models, for which the strength $\sigma_c \neq 0$ as the bundle size (N) approaches infinity. Essentially, for any finite load (σ), depending on the fiber strength distribution, the size of the defect cluster can be estimated using Lifshitz argument (see section 2.2) as $\ln N$, giving the failure strength $\sigma_c \sim 1/(\ln N)^a$, where the exponent a assumes a value appropriate for the model (see e.g., [8]). If a fraction f of the load of the failed fiber goes for global redistribution and the rest (fraction $1 - f$) goes to the fibers neighboring to the failed one, then we see (see Pradhan et al [10]) that there is a crossover from extreme to self-averaging statistics at a finite value of f .

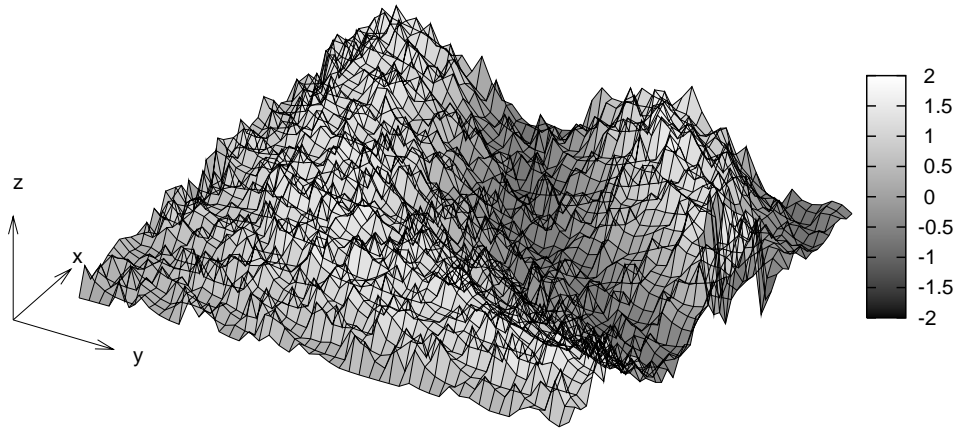


FIG. 7: A typical fracture surface: it has the self-affine scaling property $z(x; y) = z(x; y) + \lambda^D z(x/\lambda; y/\lambda)$ where the roughness exponent has some universal value (e.g., $D = 0.8$ for $(2 + 1)$ -dimensional fractured surface).

III. TWO FRACTAL OVERLAP MODEL OF EARTHQUAKE AND ITS STATISTICS

Overlapping fractals form a whole class of models to simulate earthquake dynamics. These models are motivated by the observation that a fault surface, like a fractured surface, is a fractal object [2, 3]. Consequently a fault may be viewed as a pair of overlapping fractals. Fractional Brownian profiles have been commonly used as models of fault surfaces [3]. In that case the dynamics of a fault is represented by one Brownian profile drifting on another and each intersection of the two profiles corresponds to an earthquake [20]. However the simplest possible model of a fault from the fractal point of view was proposed by Chakrabarti and Stinchcombe [17]. This model is a schematic representation of a fault by a pair of dynamically overlapping Cantor sets. It is not realistic but, as a system of overlapping fractals, it has the essential feature. Since the Cantor set is a fractal with a simple construction procedure, it allows us to study in detail the statistics of the overlap of one fractal object on another. The two fractal overlap magnitude changes in time as one fractal moves over the other. The overlap (magnitude) time series can therefore be studied as a model time series of earthquake avalanche dynamics [15].

The statistics of overlaps between two fractals is not studied much yet, though their knowledge is often required in various physical contexts. It has been established recently that since the fractured surfaces have got well-characterized self-affine properties, the distribution of the elastic energies released during the slips between two fractal surfaces (earthquake events) may follow the overlap distribution of two self-similar fractal surfaces [8, 17]. Chakrabarti and Stinchcombe [17] had shown analytically by renormalization group calculations that for regular fractal overlap (Cantor sets and carpets) the contact area distribution $\rho(s)$ follows a simple power law decay:

$$\rho(s) \sim s^{-\beta}; \quad \beta = 1: \quad (20)$$

In this so called Chakrabarti-Stinchcombe model [18], the solid-solid contact surfaces of both the earth's crust and the tectonic plate are considered as average self-similar fractal surfaces. We then consider the distribution of contact areas, as one fractal surface slides over the other. We relate the total contact area between the two surfaces to be proportional to the elastic strain energy that can be grown during the sticking period, as the solid-solid friction force arises from the elastic strains at the contacts between the asperities. We then consider this energy to be released as one surface slips over the other and sticks again to the next contact or overlap between the rough surfaces. Since the two fractured surfaces are well-known fractals, with established (self-affine) scaling properties (see Fig. 7) considering that such slips occur at intervals proportional to the length corresponding to that area, we obtain a power law for the frequency distribution of the energy releases. This compares quite well with the Gutenberg-Richter law.

In order to proceed with the estimate of the number density $n(\epsilon)$ of earthquakes releasing energy ϵ in our model, we first find out the distribution $\rho(s)$ of the overlap or contact areas between two self-similar fractal surfaces. We then relate s with ϵ and the frequency of slips as a function of s , giving finally $n(\epsilon)$. To start with a simple problem of contact area distribution between two fractals, we first take two Cantor sets [17] to model the contact area variations of two (nonrandom and self-similar) surfaces as one surface slides over the other. Figure 8 (a) depicts structure in such surfaces at a scale which corresponds to only the second generation of iterative construction of two displaced

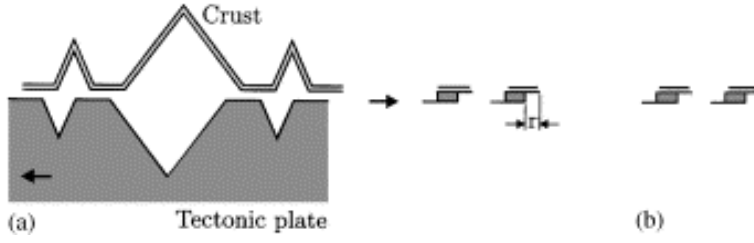


FIG .8: Schematic representations of a portion of the rough surfaces of the earth's crust and the supporting (moving) tectonic plate. (b) The one dimensional projection of the surfaces form Cantor sets of varying contacts or overlaps as one surface slides over the other.

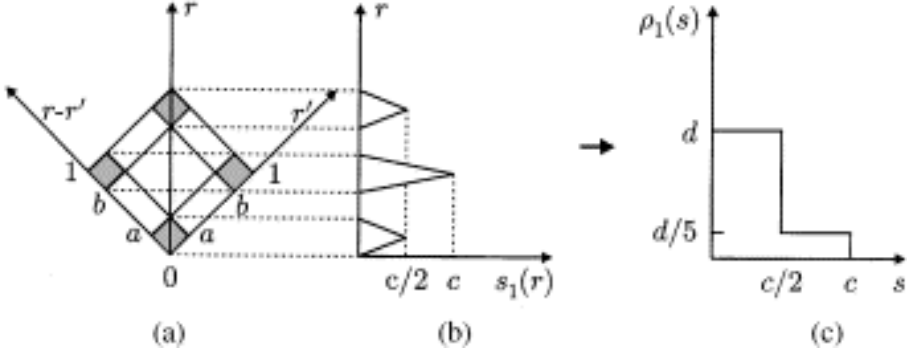


FIG .9: (a) Two cantor sets (in their first generation) along the axes r and r' . (b) This gives the overlap $s_1(r)$ along the diagonal. (c) The corresponding density $\rho_1(s)$ of the overlap s at this generation.

Cantor sets, shown in Fig. 9 (b). It is obvious that with successive iterations, these surfaces will acquire self-similarity at every length scale, when the generation number goes to infinity. We intend to study the distribution of the total overlap s (shown by the shaded regions in Fig. 9 (b)) between the two Cantor sets, in the infinite generation limit.

Let's the sequence of generators G_l define our Cantor sets within the interval $[0,1]$: $G_0 = [0;1]$; $G_1 = RG_0 = [0;a] \cup [b;1]$ (i.e., the union of the intervals $[0;a]$ and $[b;1]$); \dots ; $G_{l+1} = RG_l$; \dots . If we represent the mass density of the set G_l by $D_l(r)$, then $D_l(r) = 1$ if r is in any of the occupied intervals of G_l , and $D_l(r) = 0$ elsewhere. The required overlap magnitude between the sets at any generation l is then given by the convolution form $s_l(r) = \int dr^0 D_l(r^0) D_l(r - r^0)$. This form applies to symmetric fractals (with $D_l(r) = D_l(-r)$); in general the argument of the second D_l should be $D_l(r + r^0)$.

One can express the overlap integral s_l in the first generation by the projection of the shaded regions along the vertical diagonal in Fig. 8 (a). That gives the form shown in Fig. 8 (b). For $a = b = \frac{1}{3}$, the nonvanishing $s_1(r)$ regions do not overlap, and are symmetric on both sides with the slope of the middle curve being exactly double those on the sides. One can then easily check that the distribution $\rho_1(s)$ of overlap s at this generation is given by Fig. 8 (c), with both c and d greater than unity, maintaining the normalisation of the probability ρ_1 with $cd = 5=3$. The successive generations of the density $\rho_l(s)$ may therefore be represented by Fig. 9, where

$$\rho_{l+1}(s) = R \rho_l(s) = \frac{d}{5} \rho_l\left(\frac{s}{c}\right) + \frac{4d}{5} \rho_l\left(\frac{2s}{c}\right) \quad (21)$$

In the infinite generation limit of the renormalisation group (RG) equation, if $\rho(s)$ denotes the fixed point distribution

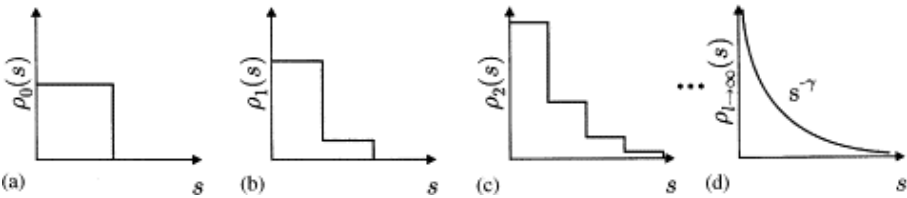


FIG .10: The overlap densities $\rho(s)$ at various generations of the Cantor sets at the zeroth (a), first (b), second (c) and at the infinite (or fixed point) (d) generations.

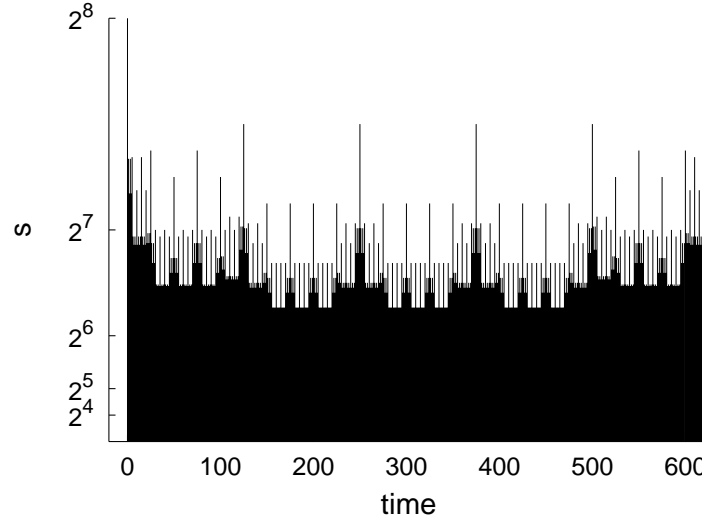


FIG . 11: For two (regular) Cantor sets, one moving uniformly over the other (with periodic boundary condition), the total measure of the (shaded region in Fig. 8 (b) contributing to the) overlap s has the time variation as shown here (for $n = 4$).

such that $\tilde{s}(s) = R^{-1}(s)$, then assuming $\tilde{s}(s) \sim s^{-\alpha}$, one gets $(d+1)\alpha + (d-1)(\alpha-2) = 1$. Here $\tilde{s}(s)$ represents an arbitrary modular function, which also includes a logarithmic correction for large s . This agrees with the above mentioned normalisation condition $\alpha d = 5=3$ for the choice $\alpha = 1$. This result for the overlap distribution (20)

$$\tilde{s}(s) \sim \frac{1}{s} ; \alpha = 1;$$

is the general result for all cases that we have investigated and solved by the functional rescaling technique (with the log s correction for large s , renormalising the total integrated distribution).

The above study is for continuous relative motion of one Cantor set over the other. Study of the time (t) variation of contact area (overlap) $s(t)$ between two well-characterized fractals having the same fractal dimension as one fractal moves over the other with constant velocity, with discrete (minimum element in that generation) steps has been studied, for finite generations [18]. Bhattacharyya [18] studied this overlap distribution for two Cantor sets with periodic boundary conditions and each having dimension $\log 2 = \log 3$ (see Fig. 11). It was shown, using exact counting, that if $s \sim 2^{n-k}$ (n is the generation number) then the probability $\tilde{s}(s)$ to get an overlap s is given by a binomial distribution [18]

$$\tilde{s}(2^{n-k}) = \binom{n}{k} \left(\frac{1}{3}\right)^{n-k} \left(\frac{2}{3}\right)^k \exp(-r^2/n); r \neq 0; \tag{22}$$

where $r^2 = \frac{3}{2} \frac{2}{3} n - k^2$. Expressing therefore r by $\log s$ near the maxima of $\tilde{s}(s)$, one can again rewrite (22) as

$$\tilde{s}(s) \sim \exp\left(-\frac{(\log s)^2}{n}\right); n \gg 1; \tag{23}$$

Noting that $\tilde{s}(s) \sim \int \tilde{s}(s) ds$, we find $\tilde{s}(s) \sim s^{-1}$, as in (20), as the binomial or Gaussian part becomes a very weak function of s as $n \gg 1$ [21]. It may be noted that this exponent value $\alpha = 1$ is independent of the dimension of the Cantor sets considered (here $\log 2 = \log 3$) or for that matter, independent of the fractals employed. It also denotes the general validity of (20) even for disordered fractals, as observed numerically [8].

Identifying the contact area or overlap s between the self-similar (fractal) crust and tectonic plate surfaces as the stored elastic energy E released during the slip, the distribution (20), of which a derivation is partly indicated here, reduces to the Gutenberg-Richter law (3) observed.

IV . S U M M A R Y A N D D I S C U S S I O N S

Unlike the elastic constants (e.g., Y in eqn. (4)) of a solid, which can be estimated from the interatomic interactions and lattice structures of a solid and while the effect of disorder on them can be accommodated using simple analytic

formulas, the fracture strength (σ_f) of a solid cannot be estimated easily from there and such estimates are orders of magnitude higher than those observed. The reason is that cracks nucleate around a defect or disorder in the solid and the variation of σ_f with the defect size l can be precisely estimated in a brittle solid using the Griffith's formula (4) in Sec. 2.1.

For disordered solids, the failure strength distribution $F(\sigma)$ depends on the sample volume and is given by the extreme statistics: Gumbel [2] or Weibull [2] type (see Fig. 2 for their generic behavior). The average strength of a (finite volume) sample can be estimated from a modified Griffith-like formula (7). When percolation correlation length exceeds the Lifshitz length, for large disorder, self-averaging statistics takes over (see Sec. 2.2) and the average strength, given by (7), becomes precisely defined (even for infinite system size) and σ_f becomes volume independent (as in the equal load sharing fiber bundle model).

The inherent mean-field nature of the equal load sharing models (discussion in Sec. 2.3) enables us to construct recursion relations (Eq. (9) for example) which captures essentially all the intriguing features of the failure dynamics. Though we have identified $O(U(\sigma) - U(\sigma_f) / (\sigma - \sigma_f))$ as the order parameter (with exponent $\nu = 1/2$) for the continuous transition in such models, unlike in the conventional phase transitions it does not have a real-valued existence for $\sigma > \sigma_f$. The 'type' of phase transition in such models has been a controversial issue. Earlier it was suggested to be a first order phase transition, because the surviving fraction of fibers has a discontinuity at the breakdown point of the bundles. However, as the susceptibility shows divergence ($\chi \sim (\sigma - \sigma_f)^{-\nu}$; $\nu = 1/2$) at the breakdown point, the transition has been later identified to be of second order [10]. The dynamic critical behavior of these models and the universality of the exponent values are straightforward. Here, divergence of relaxation time (τ) at the critical point ($\sigma \rightarrow \sigma_f$; $\nu = 1/2$) indicates 'critical slowing' of the dynamics which is characteristic of conventional critical phenomena. At the critical point, one observes power law decay of the surviving fraction in time ($U(\sigma_f) - U(\sigma) \sim t^{-\nu}$; $\nu = 1$). We demonstrated the universality of the failure behavior near $\sigma = \sigma_f$, for three different distributions: uniform, linearly increasing and linearly decreasing distributions of fiber strength. The critical strengths of the bundles differ in each case: $\sigma_f = 1/4$; $4/27$ and $4/27$ respectively for these three distributions. However, the critical behavior of the order parameter O , susceptibility, relaxation time and of the time decay at σ_f , as given by the exponents ν ; χ ; and remain unchanged: $\nu = 1/2$; $\chi = 1/2$ and $\nu = 1$ for all three distributions.

The model also shows realistic nonlinear deformation behavior with a shifted (by L , away from the origin) uniform distribution of fiber strengths (see Sec. 2.3.2). The stress-strain curve for the model clearly shows three different regions: elastic or linear part (Hooke's region) when none of the fibers break ($U(\sigma) = 1$), plastic or nonlinear part due to the successive failure of the fibers ($U(\sigma) < 1$) and then finally the stress drops suddenly (due to the discontinuous drop in the fraction of surviving fibers from $U(\sigma_f)$ to zero) at the failure point $\sigma_f = 1/[4(1 - L)]$. This nonlinearity in the response (stress-strain curve in Fig. 6) results from the linear response of the surviving fibers who share the extra load uniformly. The local load sharing bundles (see Sec. 2.3.3) on the other hand show 'zero' critical strength as the bundle size goes to infinity in one dimension (extreme statistics takes over). It is not clear at this stage if, in higher dimensions, LLS bundles are going to have non-zero critical strength. In any case, the associated dynamics of failure of these higher dimensional bundles with variable range load transfer should be interesting.

We believe, the elegance and simplicity of the model, its common-sense appeal, the exact solubility of its critical behavior in the mean-field (ELS) limit, its demonstrated universality, etc, would promote the model eventually to a level competing with the Ising model of magnetic critical behavior.

As emphasized already, we consider the physicist's identification of the Gutenberg-Richter law (3) as an extremely significant one in geophysics. Like the previous attempts [14, 15, 16], the model developed here [17] captures this important feature in its resulting statistics. Here, the established self-similarity of the fault planes are captured using fractals, Cantor sets in particular. Hence we consider, in Sec. 3, this Chakrabarti-Stinchcombe model [18], where one Cantor set moves uniformly over another similar set (with periodic boundary conditions). The resulting overlaps (meaning the set of real numbers common in both the Cantor sets) changes with time: see, for example, Fig. 11 for a typical time variation overlaps for $n = 4$. The number density of such overlaps seem to follow a Gutenberg-Richter type law (20). Judging from the comparisons of the exponent values in (3) and in (20), the model succeeds at least as well as the earlier ones. More importantly, our model incorporates both the geologically observed facts: fractal nature of the contact surfaces of the crust and of the tectonic plate, and the stick-slip motion between them. However, the origin of the power law in the quake statistics here is the self-similarity of the fractal surfaces, and not any self-organization directly in their dynamics. In fact, the extreme non-linearity in the nature of the crack propagation is responsible for the fractal nature of the rough crack surfaces of the crust and the tectonic plate. This in turn leads here to the Gutenberg-Richter like power law in the earthquake statistics.

Acknowledgments: The author thanks M. Acharya, K. K. Bardhan, L. G. Benguigui, P. Bhattacharyya, A. Chatterjee, D. Chowdhury, M. K. Dey, A. Hansen, S. S. Manna, S. Pradhan, P. Ray, D. Stauffer and R. B. Stinchcombe

for collaborations at different stages.

-
- [1] B. Lawn, *Fracture of Brittle Solids*, Cambridge Univ. Press, Cambridge (1993).
- [2] B.K. Chakrabarti and L.G. Benguigui, *Statistical Physics of Fracture and Breakdown in Disorder Systems*, Oxford Univ. Press, Oxford (1997).
- [3] H.J. Herrmann and S. Roux (Eds.) *Statistical Models for the Fracture of Disordered Media*, Elsevier, Amsterdam (1990); M. Sahimi, *Heterogeneous Materials*, Vol. II, Springer, New York (2003).
- [4] D. Stauffer and A. Aharony, *Introduction to Percolation Theory*, Taylor and Francis, London (1992).
- [5] A.A. Griffith, *Phil Trans. Roy. Soc. Lond. A* 221 163 (1920).
- [6] F.T. Pierce, *J. Textile Inst.* 17, T 355-368 (1926).
- [7] H.E. Daniels, *Proc. R. Soc. London A* 183 405 (1945); S.L. Phoenix, *SIAM J. Appl. Math.* 34 227 (1978); *Adv. Appl. Prob.* 11 153 (1979).
- [8] S. Pradhan and B.K. Chakrabarti, *Int. J. Mod. Phys. B* 17 5565 (2003).
- [9] P.C. Hemmer and A. Hansen, *J. Appl. Mech.* 59 909 (1992); M. Kloster, A. Hansen and P.C. Hemmer, *Phys. Rev. E* 56 2615 (1997); S. Pradhan, A. Hansen and P.C. Hemmer, *Phys. Rev. Lett.* 95 125501 (2005); F. Raischel, F. Kun and H. J. Herrmann, *cond-m at/0601290* (2006).
- [10] S. Pradhan and B.K. Chakrabarti, *Phys. Rev. E* 65 016113 (2001); S. Pradhan, P. Bhattacharyya and B.K. Chakrabarti, *Phys. Rev. E* 66 016116 (2002); P. Bhattacharyya, S. Pradhan and B.K. Chakrabarti, *Phys. Rev. E* 67 046122 (2003).
- [11] R.C. Hidalgo, F. Kun and H.J. Herrmann, *Phys. Rev. E* 64 066122 (2001); S. Pradhan, B.K. Chakrabarti and A. Hansen, *Phys. Rev. E* 71 036149 (2005).
- [12] B. Gutenberg and C.F. Richter, *Seismicity of the Earth and Associated Phenomena*, Princeton Univ. Press, Princeton, N.J. (1954).
- [13] L. Knopov, *Proc. Natl. Acad. Sci. USA* 97 11880 (2000); Y.Y. Kagan, *Physica D* 77 160 (1994); C.H. Scholz, *The Mechanics of Earthquake and Faulting*, Cambridge Univ. Press, Cambridge (1990); B.V. Kostrov and S. Das, *Principles of Earthquake Source Mechanics*, Cambridge Univ. Press, Cambridge (1988).
- [14] R. Burridge and L. Knopov, *Bull. Seis. Soc. Am.* 57 341-371 (1967).
- [15] J.M. Carlson and J.S. Langer, *Phys. Rev. Lett.* 62 2632-2635 (1989); J.M. Carlson, J.S. Langer and B.E. Shaw, *Rev. Mod. Phys.* 66 657-670 (1994); G. Ananthakrishna and H. Ramachandran in *Nonlinearity and Breakdown in Soft Condensed Matter*, Eds. K.K. Bardhan, B.K. Chakrabarti and A. Hansen, LNP 437, Springer Verlag, Heidelberg (1994); T. Mori and H. Kawamura, *Phys. Rev. Letts.*, 94 058501 (2005).
- [16] P. Bak, *How Nature works*, Oxford Univ. Press, Oxford (1997).
- [17] B.K. Chakrabarti and R.B. Stinchcombe, *Physica A* 270 27 (1999); S. Pradhan, B.K. Chakrabarti, P. Ray and M.K. Dey, *Phys. Scripta T* 106 77 (2003).
- [18] P. Bhattacharyya, *Physica A* 348 199 (2005).
- [19] D.J. Bergman and D. Stroud, in *Solid State Physics*, 46 Eds. H. Ehrenreich and D. Tumbull, Academic Press, New York, p.147 (1992).
- [20] V. de Rubeis, R. Hallgass, V. Loreto, G. Paladin, L. Pietronero and P. Tosi, *Phys. Rev. Lett.* 76 2599 (1996).
- [21] B.K. Chakrabarti and A. Chatterjée, in *Proc. The Seventh International Conference on Vibration Problems ICOVP-2005, Istanbul*, Ed. E. Inan (Springer, 2006), [arXiv:cond-m at/0512136](https://arxiv.org/abs/cond-m at/0512136); P. Bhattacharyya, A. Chatterjée and B.K. Chakrabarti, [arXiv:physics/0510038](https://arxiv.org/abs/physics/0510038).